

Molecular origins of enhanced bioproduct properties by pretreatment of agricultural residues with deep eutectic solvents

Yan Yu^{a,b}, Zhangmin Wan^d, Jerry M. Parks^{a,b}, Shahabaddine Sokhansanj^d, Orlando J. Rojas^{d,e,f}, and Jeremy C. Smith^{a,c*}*

^aUT/ORNL Center for Molecular Biophysics, Oak Ridge National Laboratory, Oak Ridge, Tennessee 37831, United States

^bBiosciences Division, Oak Ridge National Laboratory, Oak Ridge, Tennessee 37831, United States

^c Department of Biochemistry and Cellular and Molecular Biology, University of Tennessee, Knoxville, Tennessee 37996, United States

^d Bioproducts Institute, Department of Chemical & Biological Engineering, The University of British Columbia, 2360 East Mall, Vancouver, BC V6T 1Z3, Canada

^e Department of Chemistry, The University of British Columbia, Vancouver, BC V6T 1Z1, Canada

^f Department of Wood Science, The University of British Columbia, Vancouver, BC V6T 1Z4, Canada

*Corresponding authors: Orlando J. Rojas (orlando.rojas@ubc.ca); Jeremy C. Smith (smithjc@ornl.gov)

List of Figures

Figure S1. Experimental process used in the present study.....	7
Figure S2. Collective variables (CVs) as a function of time from a metadynamics simulation of (a) Scenario 1 and (b) Scenario 2.	8
Figure S3. Electrostatic potential (ESP) of lignin LCC and oxalic acid. Red and blue regions represent positive and negative potential, respectively.	9
Figure S4. The Laplacian of the electron density for C ^H in the marked region is positive (red), which indicates that nucleophilic attack is favorable.	10
Figure S5. Lignin distribution (a, c, e, g) and relative position information (b, d, f, h) in the XZ plane for untreated DES2-1, DES1-1, and DES1-2-treated samples from MD simulations.	11
Figure S6. Lignin distribution (a, c, e, g) and relative position information (b, d, f, h) in the YZ plane for untreated DES2-1, DES1-1, and DES1-2-treated samples from MD simulations.	12
Figure S7. Conformational (a) entropy and (b) enthalpy of lignin in different DESs.	13
Figure S8. Mayer hardness and energy density of pellets made from untreated and DES-treated wheat straw both show an increasing trend as the ratio of oxalic acid increased in DESs.	14
Figure S9. Water contact angles for pellets made from untreated and DES-treated wheat straw.	15

List of Tables

Table S1. Fukui indices for LCC.	14
Table S2. Fukui indices for the hemicellulose monomer.....	16
Table S3. Fukui indices for the lignin monomer.	17
Table S4. Pyrolysis parameters and <i>CrI</i> of different samples.....	19

Cellulose crystal model

Cellulose accounts for nearly half the mass of the cell wall. Its structure in wood cell layers has been widely investigated^{1,2}, but few studies have revealed detailed information regarding amorphous cellulose from wheat resources. Simulating the complete plant cell wall is currently challenging. However, the cellulose crystal-lignin interface in the co-solvent environment has been characterized^{3,4}. It has been reported that the stable cellulose I_{β} crystalline structure exists in wheat straw⁵. For these reasons, the cellulose I_{β} crystalline structure was used to investigate the cellulose-lignin interfaces in the corresponding DES solution environment.

A cellulose crystal model was constructed according to the corresponding crystallographic vectors: $a = 0.7784$ nm, $b = 0.8201$ nm, $c = 1.0380$ nm, and $\gamma = 96.5^\circ$ ⁶. The cellulose crystal, representing the cellulose fiber in the straw residue, was assembled with 18 cellulose chains, which is accepted as representing cellulose microfibrils⁷⁻⁹. Each cellulose chain contained 30 glucose monomers. The cellulose I_{β} crystal was described with the CHARMM36 force field¹⁰, which has been demonstrated to model cellulose and lignin accurately¹¹. The crystal structure of cellulose I_{β} was initially optimized under an NPT ensemble at ambient conditions of 1 bar and 298.15 K over a duration of 1 ns. This step was followed by further equilibration of the configuration through energy minimization, employing both the steepest descent and conjugate gradient methods, with the threshold for the maximum force set to less than 10 kJ mol⁻¹ nm⁻¹. The equilibrium crystallographic vectors for cellulose I_{β} were determined to be approximately $a = 0.792$ nm, $b = 0.8134$ nm, $c = 1.041$ nm, and $\gamma = 93.1^\circ$. The average deviation from experimental data for a , b , and c were 1.75%, 0.82%, and 0.29%, with a maximum of 3.52% for angle γ , indicating reasonable agreement between the simulation results and experimental data.

Lignin

The lignin model in this study consisted of *p*-hydroxyphenyl (H), guaiacyl (G), and syringyl (S), and the complex structure together with *p*-coumaric acid (pCA) and ferulic acid. MD was used to predict the lignin configurational statistics changes that occur in DES solutions. Previous studies have demonstrated that β -O-4 ethers (75%) are the most common covalent linkage between lignin subunits in wheat straw. NMR spectroscopy has shown that the ratios of *p*-coumaryl alcohol (H), coniferyl alcohol (G), and sinapyl alcohol (S) in wheat straw cell walls are 0.1:1:1¹². Also, hydroxycinnamic acids such as *p*-coumaric acid (pCA) and ferulic acid (FA), along with their derived esters, are integral constituents of the structure of wheat straw lignins, ranging from 0.8% to 4.4%^{13,14}. For the simulations, the construction of the wheat straw lignin was performed using the LigninBuilder tool¹⁵. This process involved the random packing of lignin particles composed of 4 H monomers, 40 G monomers and 40 S monomers, along with 2 pCA and 2 FA monomers each. Lignin molecules have been previously demonstrated to exhibit a higher affinity for the hydrophobic surface (200 planes) of crystalline cellulose than the hydrophilic surfaces ($\bar{1}10$ and 110 planes)¹⁶. Therefore, we positioned lignin on the 200 plane of the initial model of the lignin-cellulose I_β complex model. MD simulations were performed to investigate the lignin spatial evolution on the surface of the cellulose I_β crystal, representing the biomass structure inherent to wheat straw residues.

Lignin/hemicellulose complex configurations

The interactions between lignin and hemicellulose have been widely studied^{17,18}, and it has been demonstrated that in softwood the interface is dominated by non-bonded interactions. In contrast, covalent bonding has been demonstrated for wheat straw¹⁹. A compositional analysis of the LCC derived from wheat straw reveals a composition of 86.6% carbohydrate (which includes 15% glucose, 71% xylose, 11% arabinose, and 3% galactose) along with 13.4% Klason lignin²⁰.

The lignin-carbohydrate linkage for LCC is mainly made up of benzyl ether (BE)²¹, while the γ -ester linkages make up only a small fraction. Thus, a system for the ab initio simulations was constructed featuring one xylose unit, one guaiacyl unit (G), plus twelve oxalic acid (OA) molecules and six choline chloride (ChCl) molecules.

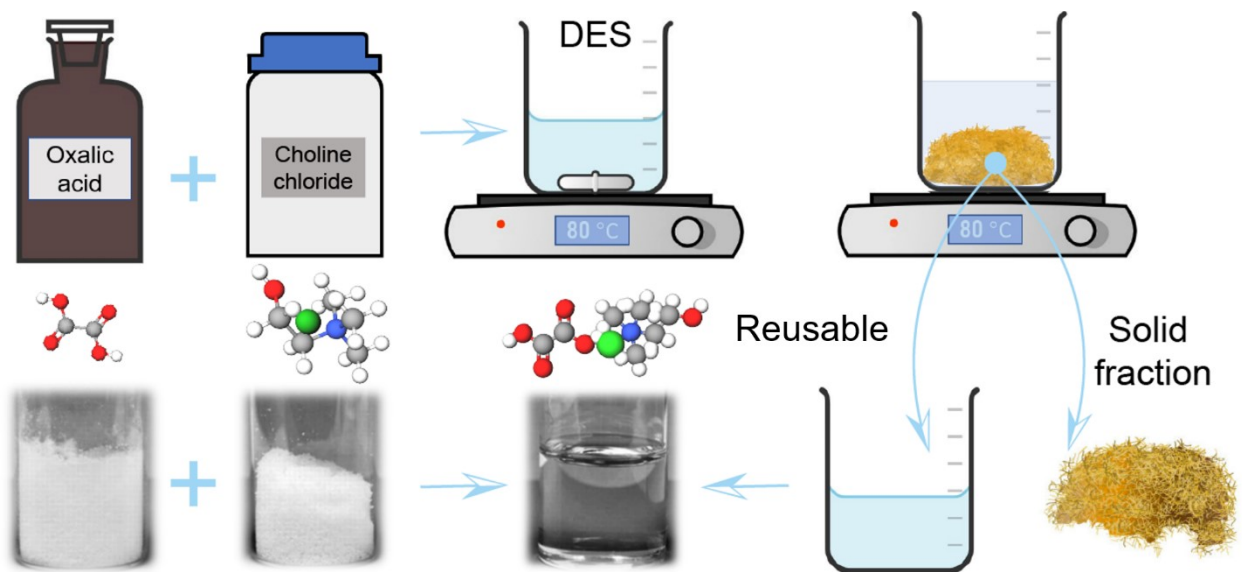


Figure S1. Experimental process used in the present study.

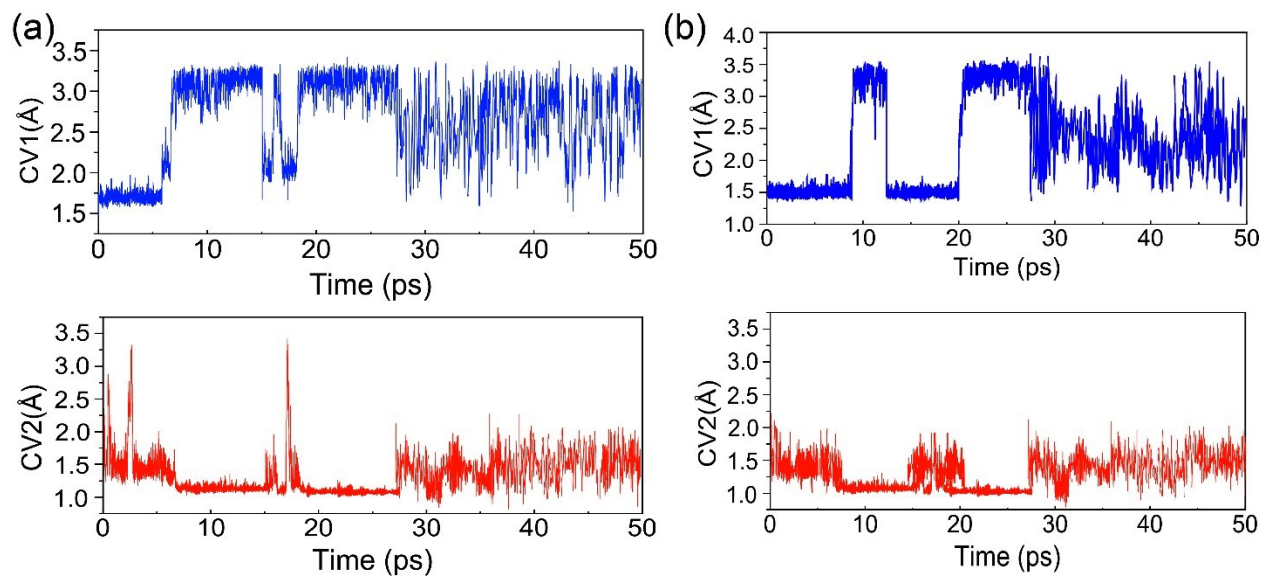


Figure S2. Collective variables (CVs) as a function of time from a metadynamics simulation of (a) Scenario 1 and (b) Scenario 2.

The molecular electrostatic potential (ESP) is of great significance for investigating electrostatic interactions between molecules, predicting reaction sites, and predicting molecular properties. A positive (negative) value implies that current position is dominated by nuclear (electronic) charges. Molecular ESP maps are highly informative for revealing charge distributions and have been widely used for predicting nucleophilic and electrophilic sites²². ESP maps were evaluated with Multiwfn 3.8 (dev)²² and rendered with VMD 1.9.3²³. Red and blue regions represent the positive and negative potential regions, respectively. The pink and green points are maximum and minimum points. The green region is the most negative region in the LCC. The region close to H^{OA} shows the most positive potential. H^{OA} could be attracted by O^{LCC}, which could help to orient the system for reaction.

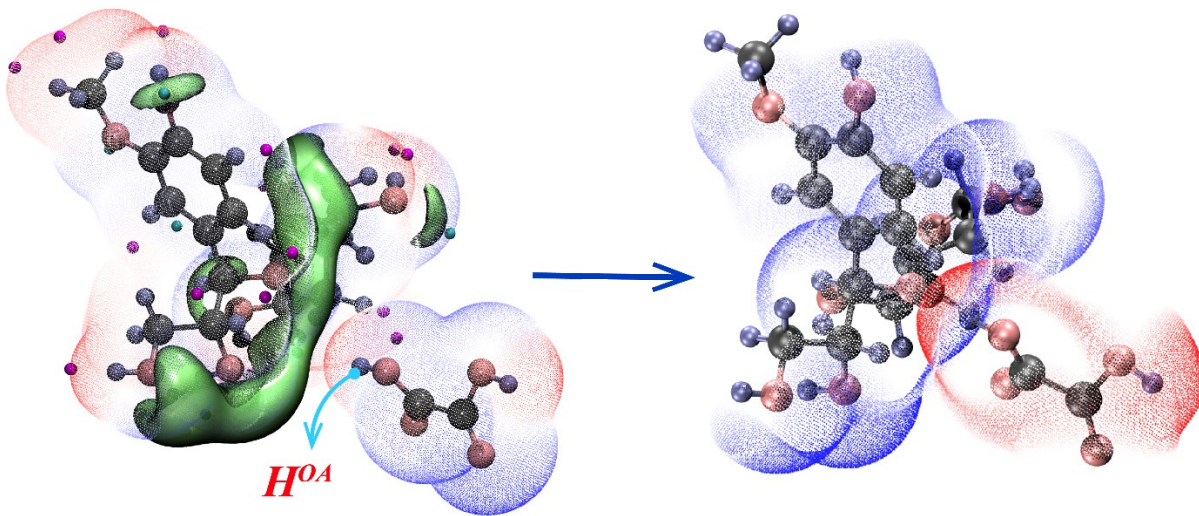


Figure S3. Electrostatic potential (ESP) of lignin LCC and oxalic acid. Red and blue regions represent positive and negative potential, respectively.

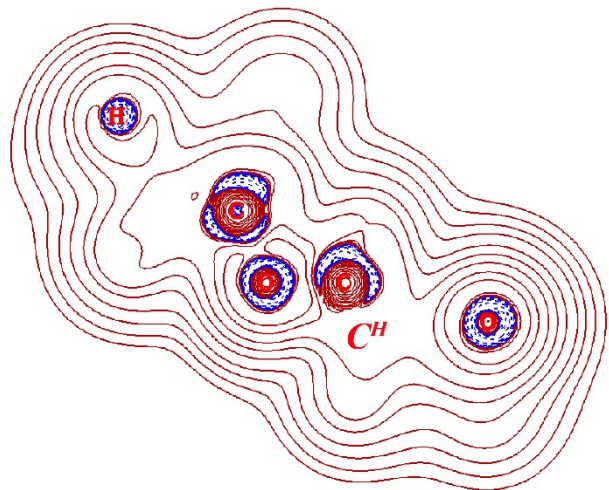


Figure S4. The Laplacian of the electron density for C^H in the marked region is positive (red), which indicates that nucleophilic attack is favorable.

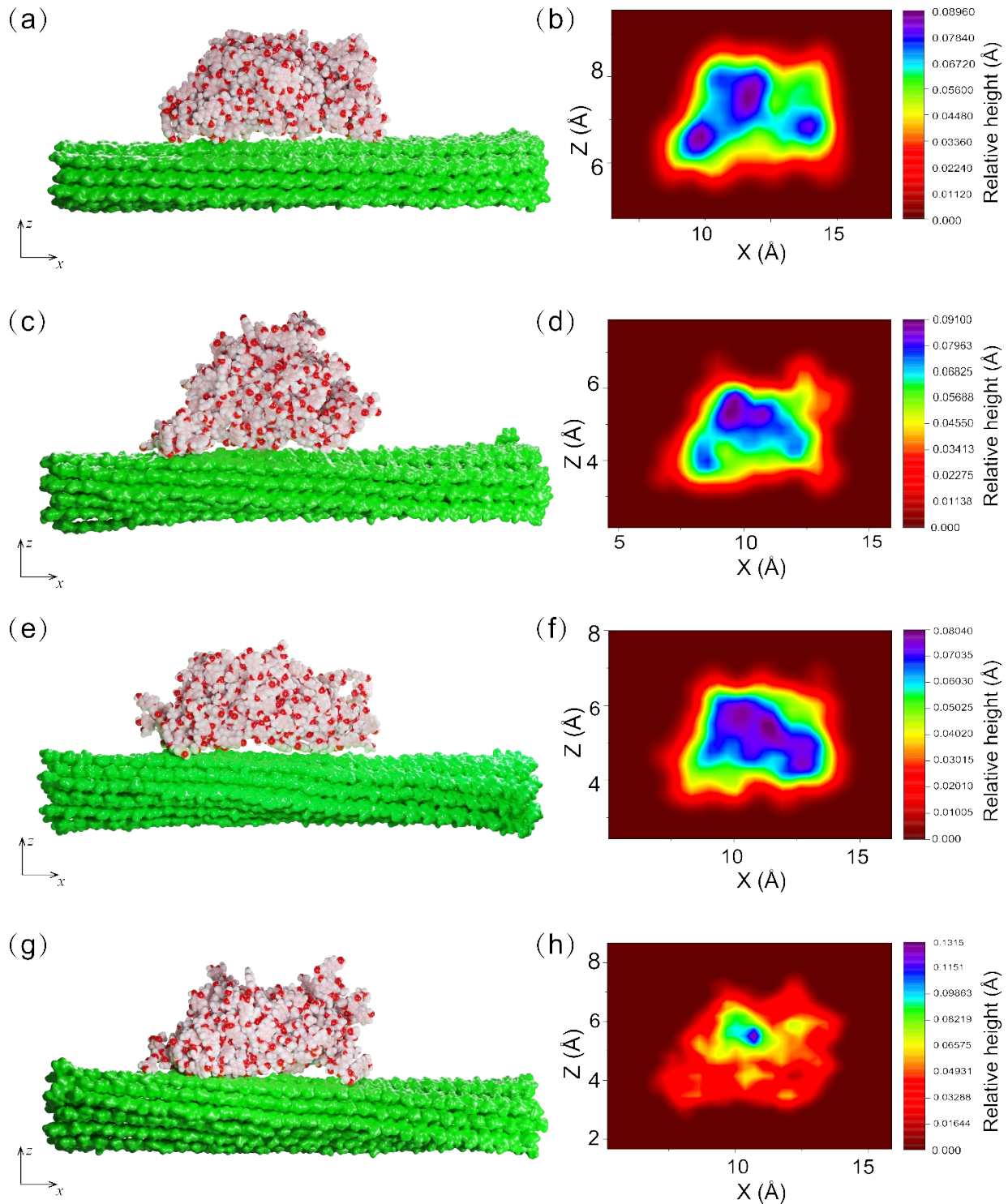


Figure S5. Lignin distribution (a, c, e, g) and relative position information (b, d, f, h) in the XZ plane for untreated DES2-1, DES1-1, and DES1-2-treated samples from MD simulations.

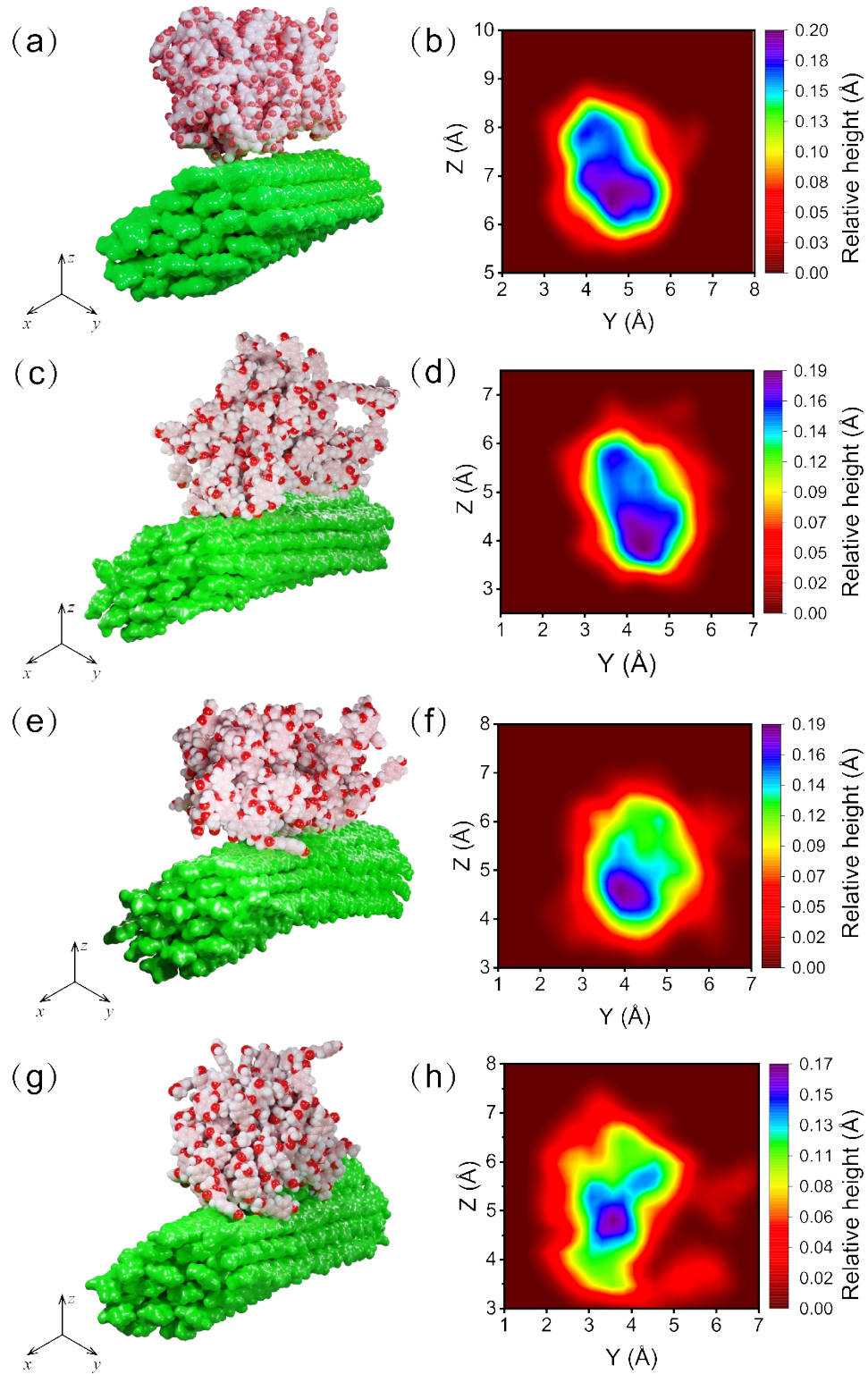


Figure S6. Lignin distribution (a, c, e, g) and relative position information (b, d, f, h) in the YZ plane for untreated DES2-1, DES1-1, and DES1-2-treated samples from MD simulations.

Entropy and enthalpy of lignin globule extension

In the context of an NPT ensemble, both enthalpic and entropic contributions play crucial roles in determining the free energy changes. **Figure S7a** and **S7b** provide the conformational entropy and enthalpy of lignin in different DESs calculated with a finite-difference approximation to predict the potential of lignin configuration changes²⁴. As the OA ratio in DES is increased, the extension of lignin globules is accompanied by a rise in lignin entropy, which leads to a decrease in the DES entropy. Ultimately, the extension of lignin results in a net increase in overall system entropy²⁵. Thus, the main driving force behind lignin extension is the increase in the entropy of the DES. DES1-2 exhibits the greatest change in conformational entropy and enthalpy among all the DESs.

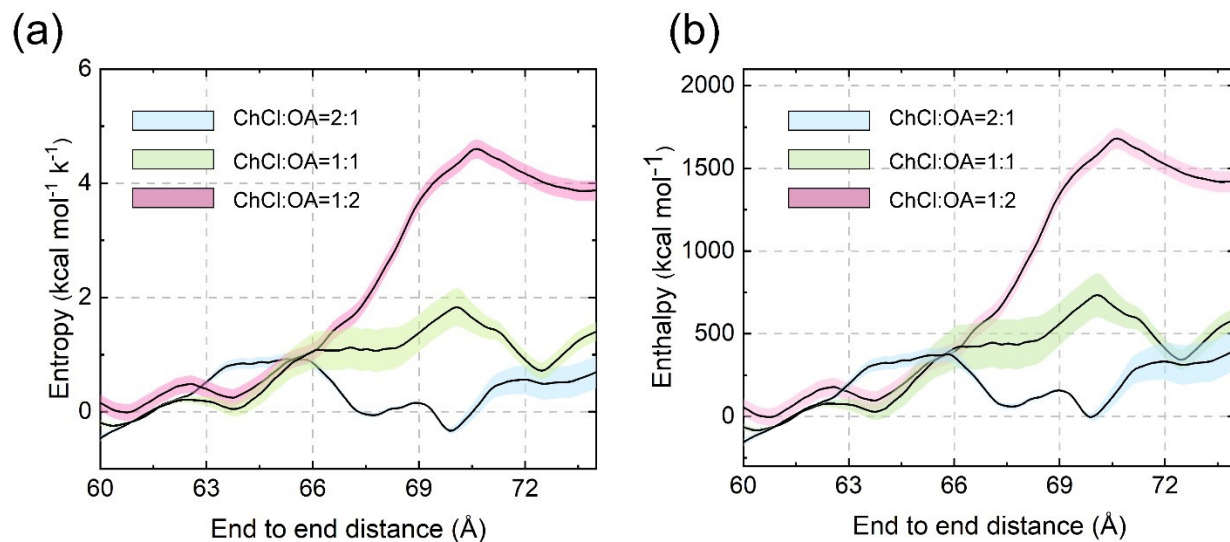


Figure S7. Conformational (a) entropy and (b) enthalpy of lignin in different DESs.

The Meyer hardness (H_M) test was carried out by placing a cylindrical pellet horizontally between two metal plates. Specific equipment and method were introduced in the previous study²⁶. The compression rate was set at 5 mm/min, and it stopped when the pellet was broken. The Meyer hardness was calculated by Eq. (1),

$$H_M = F/\pi(Dh - h^2) \quad (1)$$

where h is the indentation length (mm), D is the pellet diameter (mm), and F is the maximum force when the pellet is crushed (N).

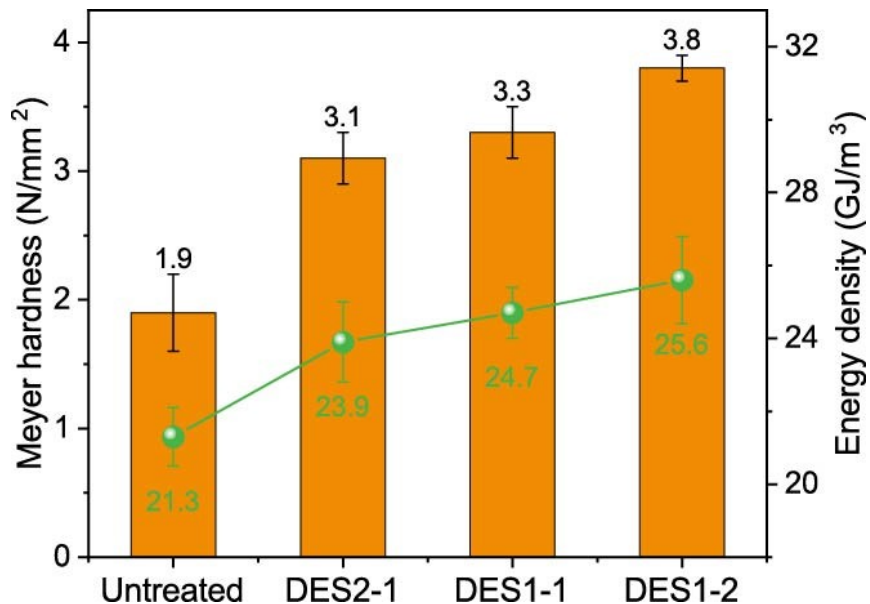


Figure S8. Mayer hardness and energy density of pellets made from untreated and DES-treated wheat straw both show an increasing trend as the ratio of oxalic acid increased in DESs.

The water contact angle on the pellet surfaces was measured using a tensiometer (Biolin, Theta Flex 300, Sweden) with a ca. 5 μm drop of distilled water on the surface of pellets.

As the ratio of oxalic acid increased in DESs, the water contacting angles of the pellets made from treated wheat straw became larger, which indicates that more OA could promote pellets made from treated wheat straw more difficult to adsorb moisture and more hydrophobic.

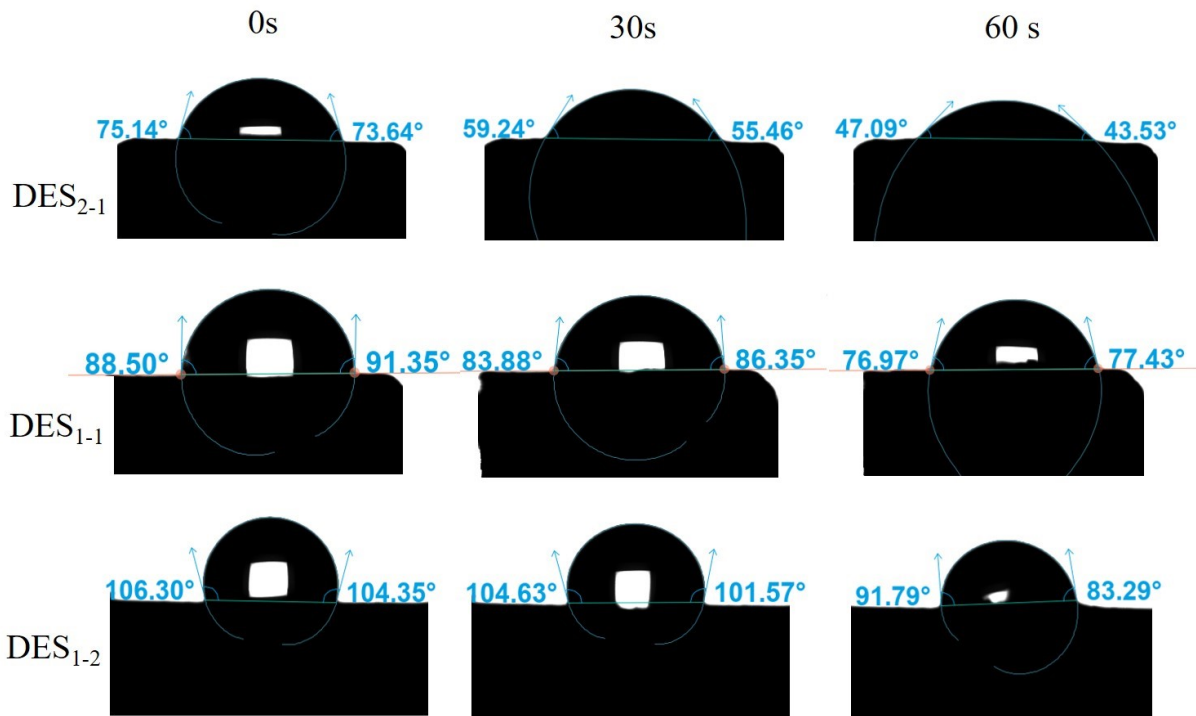


Figure S9. Water contact angles for pellets made from untreated and DES-treated wheat straw.

Table S1. Fukui indices for LCC.

Atom	$q(N)$	$q(N+1)$	$q(N-1)$	f	f^+	f^0	CDD	s^-	s^+	s^0	s^+/s^-	s^-/s^+
1 (C)	-0.0113	-0.0303	0.0444	0.0557	0.019	0.0374	-0.0367	0.1742	0.0595	0.1169	0.3418	2.9258
2 (C)	-0.0584	-0.1096	-0.0312	0.0272	0.0512	0.0392	0.024	0.0851	0.1602	0.1226	1.8835	0.5309
3 (C)	0.0516	0.0063	0.1186	0.0669	0.0454	0.0561	-0.0215	0.2092	0.1419	0.1756	0.6782	1.4744
4 (C)	0.048	0.0229	0.1227	0.0747	0.0251	0.0499	-0.0496	0.2336	0.0785	0.156	0.3359	2.9772
5 (C)	-0.0521	-0.1131	-0.0168	0.0354	0.061	0.0482	0.0256	0.1106	0.1907	0.1506	1.725	0.5797
6 (C)	-0.0437	-0.09	0.0345	0.0782	0.0463	0.0623	-0.0319	0.2446	0.1448	0.1947	0.592	1.6892
7 (H)	0.0379	0.0085	0.0647	0.0268	0.0294	0.0281	0.0026	0.0838	0.0918	0.0878	1.0952	0.9131
8 (H)	0.0413	0.0148	0.0766	0.0353	0.0264	0.0309	-0.0089	0.1105	0.0827	0.0966	0.7483	1.3364
9 (H)	0.0452	0.0107	0.0769	0.0317	0.0345	0.0331	0.0029	0.099	0.1079	0.1035	1.09	0.9174
10 (O)	-0.1309	-0.1501	-0.0593	0.0716	0.0192	0.0454	-0.0524	0.2238	0.0601	0.142	0.2686	3.7229
11 (O)	-0.1948	-0.2263	-0.1199	0.0749	0.0315	0.0532	-0.0434	0.2342	0.0986	0.1664	0.4211	2.3747
12 (H)	0.1504	0.1023	0.1791	0.0286	0.0482	0.0384	0.0195	0.0895	0.1506	0.12	1.6819	0.5946
13 (C)	0.0042	-0.019	0.0245	0.0203	0.0231	0.0217	0.0028	0.0636	0.0724	0.068	1.1383	0.8785
14 (H)	0.0474	0.0218	0.0748	0.0274	0.0256	0.0265	-0.0018	0.0857	0.08	0.0828	0.933	1.0718
15 (H)	0.0328	-0.0083	0.0543	0.0215	0.0411	0.0313	0.0196	0.0672	0.1286	0.0979	1.9147	0.5223
16 (H)	0.0387	0.0245	0.0578	0.0191	0.0142	0.0166	-0.0049	0.0597	0.0443	0.052	0.7421	1.3476
17 (C)	0.0493	0.0467	0.0565	0.0072	0.0026	0.0049	-0.0046	0.0225	0.0081	0.0153	0.3578	2.7949
18 (C)	0.0535	0.0488	0.0569	0.0034	0.0047	0.004	0.0013	0.0106	0.0147	0.0126	1.3829	0.7231
19 (C)	0.0152	0.0073	0.0172	0.002	0.0079	0.005	0.0059	0.0063	0.0247	0.0155	3.9065	0.256
20 (O)	-0.2345	-0.2522	-0.2177	0.0168	0.0177	0.0172	9E-4	0.0525	0.0552	0.0539	1.0522	0.9504
21 (H)	0.0207	0.0042	0.0289	0.0082	0.0165	0.0124	0.0084	0.0256	0.0517	0.0387	2.022	0.4946
22 (H)	0.0269	0.0197	0.0244	-0.0026	0.0072	0.0023	0.0098	-0.008	0.0227	0.0073	-2.8213	-0.3544
23 (H)	0.1561	0.1236	0.1687	0.0126	0.0325	0.0226	0.0198	0.0395	0.1016	0.0706	2.5694	0.3892
24 (O)	-0.2268	-0.2462	-0.2009	0.0259	0.0194	0.0226	-0.0065	0.0809	0.0607	0.0708	0.7495	1.3342
25 (H)	0.0426	0.0332	0.0506	0.008	0.0094	0.0087	0.0014	0.0251	0.0294	0.0273	1.1754	0.8508
26 (H)	0.1434	0.1112	0.1566	0.0132	0.0322	0.0227	0.019	0.0413	0.1008	0.071	2.4422	0.4095
27 (O)	-0.1583	-0.1639	-0.1111	0.0472	0.0056	0.0264	-0.0416	0.1475	0.0176	0.0826	0.119	8.4003
28 (H)	0.0259	0.0191	0.0403	0.0144	0.0068	0.0106	-0.0076	0.0451	0.0212	0.0332	0.4707	2.1243
29 (C)	0.0535	0.0516	0.0574	0.0039	0.0019	0.0029	-0.002	0.0122	0.006	0.0091	0.4923	2.0312
30 (C)	0.0442	0.036	0.0516	0.0074	0.0082	0.0078	8E-4	0.0231	0.0256	0.0243	1.1064	0.9038
31 (C)	0.0431	0.04	0.0442	0.0011	0.0031	0.0021	0.002	0.0035	0.0097	0.0066	2.8135	0.3554
32 (H)	0.0367	0.0337	0.0391	0.0024	0.003	0.0027	6E-4	0.0076	0.0093	0.0085	1.228	0.8143
33 (C)	0.1097	0.1031	0.1128	0.0031	0.0066	0.0048	0.0035	0.0097	0.0206	0.0151	2.1286	0.4698

34 (O)	-0.1763	-0.1841	-0.1593	0.017	0.0077	0.0124	-0.0093	0.0533	0.0242	0.0387	0.4545	2.2003
35 (O)	-0.2204	-0.2211	-0.2254	-0.005	7E-4	-0.0022	0.0057	-0.0157	0.0021	-0.0068	-0.1366	-7.3224
36 (H)	0.0336	0.0232	0.0422	0.0086	0.0105	0.0095	0.0019	0.0268	0.0327	0.0298	1.2226	0.8179
37 (H)	0.1535	0.1333	0.1648	0.0113	0.0202	0.0158	0.0089	0.0353	0.0632	0.0493	1.7876	0.5594
38 (O)	-0.2315	-0.2518	-0.2198	0.0116	0.0203	0.016	0.0087	0.0363	0.0636	0.05	1.753	0.5705
39 (H)	0.0313	0.0215	0.0348	0.0035	0.0098	0.0066	0.0063	0.0109	0.0306	0.0208	2.8014	0.357
40 (H)	0.1586	0.1072	0.1697	0.0111	0.0515	0.0313	0.0404	0.0346	0.1609	0.0977	4.6533	0.2149
41 (C)	0.0176	0.0062	0.0289	0.0113	0.0115	0.0114	1E-4	0.0354	0.0358	0.0356	1.0112	0.989
42 (H)	0.0399	0.0158	0.0541	0.0142	0.0241	0.0191	0.01	0.0443	0.0754	0.0599	1.7031	0.5872
43 (H)	0.0306	0.014	0.0425	0.0119	0.0166	0.0143	0.0047	0.0372	0.052	0.0446	1.3981	0.7153
44 (O)	-0.2276	-0.2438	-0.2171	0.0105	0.0162	0.0133	0.0057	0.0329	0.0506	0.0417	1.5391	0.6497
45 (H)	0.0316	0.0144	0.0412	0.0096	0.0172	0.0134	0.0075	0.0301	0.0536	0.0419	1.7846	0.5604
46 (H)	0.1511	0.084	0.1659	0.0148	0.0671	0.041	0.0523	0.0463	0.2098	0.1281	4.5362	0.2204

Hirshfeld charges (q), condensed Fukui functions (f) and condensed dual descriptors (CCD) (Units are "e" (elementary charge)); Condensed local softness (hartree*e) ($s^+(r) = Sf^+(r)$, $s^-(r) = Sf^-(r)$, $s^0(r) = Sf^0(r)$) and relative electrophilicity/nucleophilicity.

E(N)	-1261.590703 hartree
E(N+1)	-1261.544983 hartree
E(N-1)	-1261.316599 hartree
E_HOMO(N)	-0.212665 hartree
E_HOMO(N+1)	0.089251 hartree
E_HOMO(N-1)	-0.362181 hartree
Vertical IP	0.274104 hartree
Vertical EA	-0.045720 hartree
Mulliken electronegativity	0.114192 hartree
Chemical potential	-0.114192 hartree
Hardness (=fundamental gap)	0.319824 hartree
Softness	3.126724 hartree ⁻¹

Table S2. Fukui indices for the hemicellulose monomer.

Atom	q (N)	q (N+1)	q (N-1)	f	f ⁺	f ⁰	CDD	s ⁻	s ⁺	s ⁰	s ^{+/s⁻}	s ^{-/s⁺}
1 (C)	0.219	-0.018	0.2772	0.0582	0.237	0.1476	0.1788	0.2606	1.0607	0.6606	4.0703	0.2457
2 (C)	0.0834	0.0442	0.1182	0.0349	0.0392	0.037	0.0043	0.1561	0.1753	0.1657	1.1233	0.8902
3 (C)	0.0766	0.0382	0.0885	0.012	0.0384	0.0252	0.0264	0.0536	0.1717	0.1126	3.2051	0.312
4 (H)	0.1165	0.0403	0.1412	0.0246	0.0762	0.0504	0.0516	0.1102	0.3411	0.2257	3.0938	0.3232
5 (C)	0.1491	0.1121	0.175	0.026	0.037	0.0315	0.011	0.1163	0.1657	0.141	1.4245	0.702
6 (O)	-0.1272	-0.1739	0.0369	0.164	0.0467	0.1054	-0.1173	0.7342	0.2092	0.4717	0.285	3.5088
7 (O)	-0.1696	-0.229	-0.1083	0.0613	0.0593	0.0603	-0.002	0.2745	0.2656	0.27	0.9675	1.0336
8 (H)	0.0744	0.0297	0.0994	0.025	0.0447	0.0348	0.0198	0.1117	0.2001	0.1559	1.7914	0.5582
9 (H)	0.1896	0.1527	0.216	0.0264	0.0369	0.0316	0.0105	0.1182	0.165	0.1416	1.3961	0.7163
10 (O)	-0.1881	-0.2309	-0.0857	0.1024	0.0428	0.0726	-0.0597	0.4584	0.1914	0.3249	0.4176	2.3949
11 (H)	0.0648	0.0333	0.0997	0.0349	0.0315	0.0332	-0.0034	0.1562	0.141	0.1486	0.9023	1.1083
12 (H)	0.1968	0.1601	0.2354	0.0386	0.0367	0.0376	-0.0019	0.1726	0.1642	0.1684	0.9514	1.0511
13 (C)	0.0657	0.0211	0.1061	0.0404	0.0446	0.0425	0.0042	0.1807	0.1995	0.1901	1.1036	0.9062
14 (H)	0.0889	0.043	0.1222	0.0334	0.0458	0.0396	0.0125	0.1493	0.2051	0.1772	1.3737	0.728
15 (H)	0.0604	0.0298	0.1229	0.0625	0.0306	0.0466	-0.0319	0.2798	0.1371	0.2085	0.4899	2.0411
16 (O)	-0.1825	-0.2326	-0.0187	0.1637	0.0501	0.1069	-0.1136	0.7328	0.2242	0.4785	0.306	3.2678
17 (H)	0.094	0.029	0.1335	0.0395	0.0649	0.0522	0.0254	0.1769	0.2907	0.2338	1.6435	0.6085
18 (H)	0.1881	0.1505	0.2404	0.0522	0.0376	0.0449	-0.0146	0.2337	0.1683	0.201	0.7202	1.3885

E(N)	-496.364583 hartree
E(N+1)	-496.682002 hartree
E(N-1)	-495.823748 hartree
E_HOMO(N)	-0.463952 hartree
E_HOMO(N+1)	-0.237016 hartree
E_HOMO(N-1)	-0.654598 hartree
Vertical IP	0.540835 hartree
Vertical EA	0.317419 hartree
Mulliken electronegativity	0.429127 hartree
Chemical potential	-0.429127 hartree
Hardness (=fundamental gap)	0.223416 hartree
Softness	4.475947 hartree ⁻¹

Table S3. Fukui indices for the lignin monomer.

Atom	q (N)	q (N+1)	q (N-1)	f	f ⁺	f ⁰	CDD	s ⁻	s ⁺	s ⁰	s ^{+/s⁻}	s ^{-/s⁺}	s ⁻
1 (C)	0.0287	-0.0108	0.0448	0.016	0.0396	0.0278	0.0235	0.0849	0.2093	0.1471	2.4652	0.4056	0.0849
2 (C)	-0.0098	-0.0541	0.053	0.0629	0.0443	0.0536	-0.0186	0.3327	0.2343	0.2835	0.7042	1.42	0.3327
3 (C)	0.0921	0.0549	0.1476	0.0555	0.0371	0.0463	-0.0184	0.2939	0.1964	0.2451	0.6684	1.496	0.2939
4 (C)	0.1317	0.052	0.1585	0.0268	0.0797	0.0532	0.0529	0.1418	0.4215	0.2816	2.9735	0.3363	0.1418
5 (C)	-0.0092	-0.0521	0.0286	0.0378	0.0429	0.0403	0.0051	0.1999	0.227	0.2134	1.1356	0.8806	0.1999
6 (C)	0.0123	-0.0469	0.0666	0.0543	0.0592	0.0567	0.0049	0.2872	0.3132	0.3002	1.0905	0.917	0.2872
7 (H)	0.0689	0.0402	0.0959	0.027	0.0287	0.0278	0.0017	0.1427	0.1519	0.1473	1.0641	0.9398	0.1427
8 (H)	0.0731	0.0414	0.1014	0.0282	0.0317	0.03	0.0035	0.1494	0.1677	0.1585	1.1223	0.8911	0.1494
9 (H)	0.0803	0.047	0.1083	0.028	0.0334	0.0307	0.0053	0.1482	0.1765	0.1624	1.1909	0.8397	0.1482
10 (O)	-0.0996	-0.1286	0.0147	0.1143	0.029	0.0717	-0.0853	0.6047	0.1535	0.3791	0.2538	3.9396	0.6047
11 (O)	-0.1216	-0.1906	-0.0739	0.0477	0.0691	0.0584	0.0214	0.2522	0.3653	0.3088	1.4486	0.6903	0.2522
12 (H)	0.1823	0.1523	0.1992	0.0169	0.03	0.0234	0.013	0.0895	0.1585	0.124	1.7711	0.5646	0.0895
13 (C)	0.0181	0.0051	0.0492	0.0311	0.013	0.0221	-0.0181	0.1646	0.0689	0.1168	0.4188	2.3879	0.1646
14 (H)	0.0716	0.0491	0.1008	0.0292	0.0225	0.0259	-0.0067	0.1546	0.1191	0.1369	0.77	1.2987	0.1546
15 (H)	0.0474	0.0338	0.0821	0.0347	0.0136	0.0241	-0.0211	0.1835	0.0719	0.1277	0.3915	2.554	0.1835
16 (H)	0.0502	0.0395	0.0808	0.0307	0.0107	0.0207	-0.02	0.1623	0.0565	0.1094	0.3479	2.8745	0.1623
17 (C)	0.1303	-0.0341	0.1822	0.0519	0.1644	0.1081	0.1124	0.2747	0.8696	0.5721	3.1652	0.3159	0.2747
18 (C)	0.0746	0.0497	0.0883	0.0137	0.0249	0.0193	0.0112	0.0726	0.1319	0.1022	1.8164	0.5505	0.0726
19 (C)	0.0363	0.016	0.0579	0.0216	0.0203	0.0209	-0.0012	0.114	0.1076	0.1108	0.9439	1.0594	0.114
20 (O)	-0.2047	-0.2341	-0.1231	0.0816	0.0294	0.0555	-0.0522	0.4315	0.1556	0.2936	0.3607	2.7727	0.4315
21 (H)	0.0372	0.0202	0.0626	0.0254	0.017	0.0212	-0.0084	0.1345	0.0902	0.1124	0.6705	1.4914	0.1345
22 (H)	0.0343	0.026	0.0453	0.011	0.0082	0.0096	-0.0028	0.0584	0.0434	0.0509	0.7436	1.3447	0.0584
23 (H)	0.1808	0.1564	0.2125	0.0317	0.0244	0.028	-0.0073	0.1678	0.129	0.1484	0.7692	1.3001	0.1678
24 (O)	-0.204	-0.2366	-0.142	0.062	0.0326	0.0473	-0.0294	0.3282	0.1726	0.2504	0.5258	1.9017	0.3282
25 (H)	0.0635	0.0395	0.0801	0.0166	0.0241	0.0203	0.0075	0.0876	0.1273	0.1074	1.4537	0.6879	0.0876
26 (H)	0.1631	0.1439	0.1851	0.022	0.0191	0.0206	-0.0029	0.1166	0.1013	0.109	0.8686	1.1513	0.1166
27 (O)	0.0722	0.0211	0.0935	0.0213	0.0512	0.0362	0.0299	0.1125	0.2707	0.1916	2.4061	0.4156	0.1125

E(N)	-689.287253 hartree
E(N+1)	-689.558404 hartree
E(N-1)	-688.827086 hartree
E_HOMO(N)	-0.398481 hartree
E_HOMO(N+1)	-0.205094 hartree
E_HOMO(N-1)	-0.547450 hartree
Vertical IP	0.460167 hartree
Vertical EA	0.271151 hartree
Mulliken electronegativity	0.365659 hartree
Chemical potential	-0.365659 hartree
Hardness (=fundamental gap)	0.189017 hartree
Softness	5.290538 hartree ⁻¹

Table S4. Pyrolysis parameters and CrI for various samples.

Samples	CrI (%)	T_{in} (°C)	T_{max} (°C)	R_{max} (%/min)	$\Delta T_{1/2}$ (°C)	D_i (10^{-6} % min ⁻¹ °C ⁻³)
WS	45.8	240.9	302.8	15.1	63.8	3.3
DES ₁₋₂	52.1	222.6	312.1	17.1	40.9	6.0
DES ₁₋₁	56.1	222.5	319.4	17.5	38.8	6.3
DES ₂₋₁	59.2	230.2	323.0	19.0	33.8	7.6

To mitigate any possible confusion for the reader we have listed the differences between our current work and previous work (“Energy pellets from whole-wheat straw processed with a deep eutectic solvent: A comprehensive thermal, molecular and environmental evaluation”) in detail:

The paper “Energy pellets from whole-wheat straw processed with a deep eutectic solvent: A comprehensive thermal, molecular and environmental evaluation” was a preliminary study by our group to demonstrate the potential of DES-treated wheat straw for solid biofuel production. This previous work focused on the physicochemical characteristics of pellets, while our current study aims to elucidate the mechanisms involved during DES pretreatment. The main differences are outlined below:

1. Original Materials for Pellets: The previous study used a mixture of raw grounded straw and DES-treated straw powder in weight ratios of 25:75 and 50:50 (DES-treated straw: raw straw). The six different pellets were made from two mixing ratios (25:75 and 50:50 for DES-treated straw) and three OA:ChCl ratios. In contrast, our current work uses pure DES-treated wheat straw to make the pellets directly without mixing with raw material.

2. Improvement of Equilibrium Moisture Content in Current Work: The current study aims to comprehensively improve pellet quality. Pure DES-treated wheat straw was used because the previous mixed pelletization did not show significant differences ($p>0.05$), especially for OA1P1 and OA2P1, where equilibrium moisture contents were 14.1% and 13.9%, respectively. Our current work demonstrates that the equilibrium moisture contents for DES2-1, DES1-1, and DES1-2 pellets are 13%, 12%, and 11%, respectively, representing a reduction of at least 20% compared to the previous mixed pellets. This also explains the difference between Fig. 7c in our current and previous work.

3. Molecular Dynamics Simulations: The methods and objectives for molecular dynamics simulations differ between the studies. The previous work obtained "lignin extension" on the cellulose surface by applying shear stress, shown in Fig. 5a, which simulated the pelletization process where pressing induces extra shear strain in lignin. Our current work simulates the DES pretreatment process without extra force, indicating automatic lignin extension during DES treatment. Fig. 5 in the current work represents the DES pretreatment process, preceding pelletization.

References:

- 1 K. Kulasinski, R. Guyer, D. Derome and J. Carmeliet, *Biomacromolecules*, 2015, **16**, 2972–2978.
- 2 D. Sawada, Y. Nishiyama, T. Röder, L. Porcar, H. Zahra, M. Trogen, H. Sixta and M. Hummel, *Polymer (Guildf.)*, 2021, **218**, 123510.
- 3 S. V. Pingali, M. D. Smith, S. H. Liu, T. B. Rawal, Y. Pu, R. Shah, B. R. Evans, V. S. Urban, B. H. Davison, C. M. Cai, A. J. Ragauskas, H. M. O'Neill, J. C. Smith and L. Petridis, *Proc. Natl. Acad. Sci. U. S. A.*, 2020, **117**, 16776–16781.
- 4 A. S. Patri, B. Mostofian, Y. Pu, N. Ciuffone, M. Soliman, M. D. Smith, R. Kumar, X. Cheng, C. E. Wyman, L. Tetard, A. J. Ragauskas, J. C. Smith, L. Petridis and C. M. Cai, *J. Am. Chem. Soc.*, 2019, **141**, 12545–12557.
- 5 R. Liu, H. Yu and Y. Huang, *Cellul. 2005* **121**, 2005, **12**, 25–34.
- 6 Y. Nishiyama, P. Langan and H. Chanzy, *Dtsch. Chem. Ges.*, 1913, **7**, 9074–9082.
- 7 V. G. Vandavasi, D. K. Putnam, Q. Zhang, L. Petridis, W. T. Heller, B. Tracy Nixon, C. H. Haigler, U. Kalluri, L. Coates, P. Langan, J. C. Smith, J. Meiler and H. O'Neill, *Plant Physiol.*, 2016, **170**, 123–135.
- 8 R. H. Newman, S. J. Hill and P. J. Harris, *Plant Physiol.*, 2013, **163**, 1558–1567.
- 9 T. Wang and M. Hong, *J. Exp. Bot.*, 2016, **67**, 503–514.
- 10 O. Guvench, S. S. Mallajosyula, E. P. Raman, E. Hatcher, K. Vanommeslaeghe, T. J. Foster, F. W. Jamison and A. D. Mackerell, *J. Chem. Theory Comput.*, 2011, **7**, 3162–3180.
- 11 T. Guo, Y. Yu, Z. Wan, S. Zargar, J. Wu, R. Bi, S. Sokhansanj, Q. Tu and O. J. Rojas, *Renew. Energy*, 2022, **194**, 902–911.
- 12 L. Zhang, A. Larsson, A. Moldin and U. Edlund, *Ind. Crops Prod.*, 2022, **187**, 115432.
- 13 R. Sun, J. M. Lawther and W. B. Banks, *Ind. Crops Prod.*, 1997, **6**, 1–8.
- 14 R.-C. Sun, X.-F. Sun and S.-H. Zhang, *J. Agric. Food Chem.*, 2001, **49**, 5122–5129.
- 15 J. V. Vermaas, L. D. Dellon, L. J. Broadbelt, G. T. Beckham and M. F. Crowley, *ACS Sustain. Chem. Eng.*, 2019, **7**, 3443–3453.
- 16 J. V. Vermaas, M. F. Crowley and G. T. Beckham, *ACS Sustain. Chem. Eng.*, 2019, **7**, 19570–19583.
- 17 A. Kirui, W. Zhao, F. Deligey, H. Yang, X. Kang, F. Mentink-Vigier and T. Wang, *Nat.*

- Commun.*, 2022, **13**, 1–12.
- 18 O. M. Terrett, J. J. Lyczakowski, L. Yu, D. Iuga, W. T. Franks, S. P. Brown, R. Dupree
and P. Dupree, *Nat. Commun.*, 2019, **10**, 1–12.
- 19 D. Tarasov, M. Leitch and P. Fatehi, *Biotechnol. Biofuels*, 2018, **11**, 269.
- 20 F. Zikeli, T. Ters, K. Fackler, E. Srebotnik and J. Li, *Ind. Crops Prod.*, 2016, **85**, 309–317.
- 21 L. Yao, C. Chen, X. Zheng, Z. Peng, H. Yang, Y. X.- BioResources and undefined 2016,
ojs.cnr.ncsu.edu, **11**, 6692–6707.
- 22 T. Lu and F. Chen, , DOI:10.1002/jcc.22885.
- 23 W. Humphrey, A. Dalke and K. Schulten, *J. Mol. Graph.*, 1996, **14**, 33–38.
- 24 H. Fu, X. Shao, W. Cai and C. Chipot, *Acc. Chem. Res.*, 2019, 3254–3264.
- 25 P. Chen, Y. Nishiyama, J. Wohlert, A. Lu, K. Mazeau and A. E. Ismail, *J. Phys. Chem. B*,
2017, **121**, 2244–2251.
- 26 P. S. Lam, S. Sokhansanj, X. Bi, C. J. Lim and S. Melin, *Energy and Fuels*, 2011, **25**,
1521–1528.